applied sciences

MDPI

Article

Beyond Time to Collision: The Point of No Return as a Reliable Safety Indicator in Rear-End Vehicle Conflicts

Adrian Soica

Department of Automotive and Transport Engineering, Transilvania University of Brasov, 500036 Brasov, Romania; a.soica@unitbv.ro

Abstract

This paper introduces the concept of the Point of No Return as a physically grounded safety indicator for rear-end vehicle conflicts, addressing fundamental limitations of the widely used time-to-collision metric. Unlike purely kinematic approaches, the proposed formulation incorporates braking capability and reaction constraints, enabling a direct assessment of whether a collision can still be avoided. To illustrate the applicability of the concept, a vision-based framework using a single camera is developed based on dashcam data, combining YOLO-based object detection, Kalman-filter tracking, and geometric distance estimation derived from bounding-box features and camera projection models. The estimated distance is further processed to obtain relative motion, allowing a unified analysis of time to collision and the Point of No Return within the same evaluation pipeline. Experimental results on real-world driving sequences show that the Point of No Return consistently precedes critical conditions identified by time to collision and provides a more stable and physically interpretable characterization of the transition toward collision inevitability. The results also highlight the sensitivity of the proposed indicator to braking capability, while showing lower sensitivity to variations in relative speed. Overall, this study demonstrates the relevance of the Point of No Return as a complementary indicator for collision risk assessment, offering a physically meaningful basis for decision-making in driver assistance systems and improving the interpretation of critical traffic situations. The proposed approach supports sustainable urban mobility by enabling earlier and more reliable intervention strategies, contributing to improved traffic safety, smoother traffic flow, and reduced environmental impact.

Keywords: Point of No Return; TTC; collision avoidance; rear end; ADAS; monocular vision; bounding box; vehicle tracking; sustainable urban mobility

Academic Editor: Suchao Xie

Received: 28 March 2026
Revised: 14 April 2026
Accepted: 14 April 2026
Published: 16 April 2026

1. Introduction

Road traffic collisions remain one of the leading causes of injury and mortality worldwide. In recent years, advanced driver assistance systems (ADASs) have been increasingly deployed to mitigate crash risk through early detection of hazardous situations and automated braking interventions.

Many of these systems rely on predictive indicators that estimate the likelihood of an impending collision. A comprehensive review of AEB technologies, covering perception, decision-making, and control subsystems, can be found in [1]. Among these indicators, time to collision (TTC) has become one of the most widely used metrics in collision risk assessment and driver assistance algorithms. Under laboratory conditions, study [2] shows that drivers can reasonably estimate time to collision only when the angular expansion

rate of the lead vehicle exceeds a perceptual threshold. However, for small TTC values, estimation errors increase significantly, leading to high variabilities and potential misjudgement of collision risk. Another paper shows that drivers initiate braking when TTC reaches a critical threshold and subsequently maintain a nearly constant braking time headway. This suggests that driver behaviour is governed by implicit safety thresholds rather than continuous distance-based control [3]. In [4], the authors demonstrate that visual estimation of TTC is prone to significant errors in the presence of acceleration, as humans tend to neglect acceleration cues. However, the addition of auditory information improves TTC estimation accuracy by enabling better perception of dynamic motion changes. While TTC is widely used to identify hazardous situations, another study demonstrates that the transition from safe to dangerous conditions is better characterized by the rate of change of TTC, named TTCD, which captures the dynamic evolution of collision risk [5]. Existing approaches attempt to enhance TTC-based automated emergency braking (AEB) by incorporating target acceleration; however, such quantities are difficult to estimate reliably in practice, whereas the proposed Point of No Return (PONR) formulation relies only on observable relative motion and braking capability, making it more reliable for real-world deployment [6].

Time to collision represents the estimated time remaining before two vehicles collide if their current relative motion remains unchanged. Due to its intuitive interpretation and computational simplicity, it has been extensively used in driver warning systems, traffic safety analysis, and AEB algorithms. A bibliographic search conducted in the Web of Science database reveals the widespread use of this indicator: The keywords "Time To Collision" and "Vehicle Collisions" return more than 12,000 publications, with more than 5000 papers published in the last five years alone (Figure 1). This highlights the central role of TTC in contemporary research on collision risk prediction.

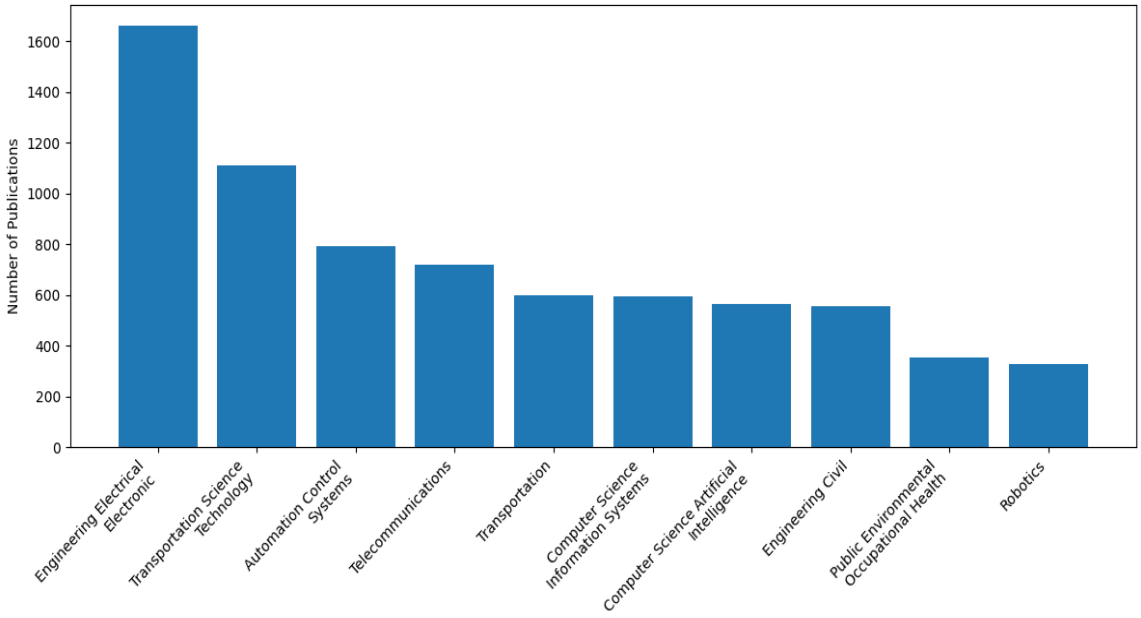

Figure 1. TTC publications in research areas from 2022 to 2026.

A concept that directly addresses this limitation is the PONR. In the context of vehicle safety, it can be defined as the critical moment or distance beyond which a collision becomes physically unavoidable even under maximum braking conditions. While the term "Point of No Return" AND "vehicle collisions" is explicitly mentioned only in [7] within the Web of Science database, reflecting its lack of formal standardization in the automotive field, the underlying concept is addressed in the literature under related keywords. These include

"inevitable collision state" AND "vehicle collisions" (51 titles), "critical braking distance" AND "vehicle collisions" (80 titles), and "brake intervention threshold" AND "vehicle collisions" (eight papers). These concepts describe the transition between avoidable and unavoidable collision conditions, typically determined by the relationship between vehicle speed, reaction time, and braking capability.

From a conceptual perspective, these two metrics represent two complementary safety indicators. While TTC estimates when an impact may occur, PONR determines whether the collision can still be avoided. In this sense, it introduces a physically meaningful threshold into accident risk assessment by explicitly considering braking dynamics and vehicle limitations.

A conceptual representation of ADAS intervention thresholds is presented in Figure 2. It shows vehicle–obstacle distance decreasing over time, with the AEB warning threshold crossed first at a higher distance, then the braking threshold, and PONR as the final unavoidable collision line, reflecting conservative TTC triggers before the true no-escape point.

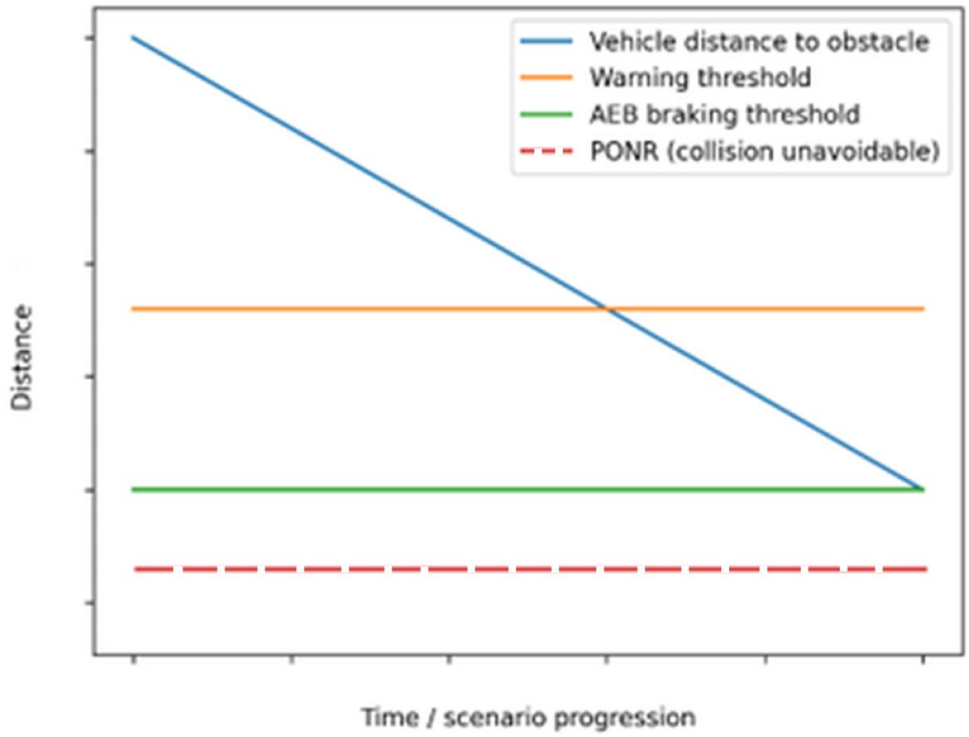

Figure 2. Conceptual ADAS intervention thresholds leading to PONR.

Despite the extensive use of time to collision as a standard indicator in collision risk assessment and ADAS, existing approaches remain predominantly kinematic and do not explicitly account for the physical feasibility of collision avoidance. As a result, TTC-based methods are limited in their ability to distinguish between avoidable and unavoidable collision states. Several studies have attempted to enhance TTC-based frameworks by incorporating additional factors such as target acceleration or dynamic thresholds. However, these approaches often rely on quantities that are difficult to estimate reliably in real-world conditions or remain indirectly related to the underlying physical constraints of braking.

At the same time, concepts related to collision inevitability have been discussed in the literature but lack a unified, operational formulation that can be directly applied within perception-driven safety frameworks. There is a lack of a physically interpretable indicator that can be derived from observable quantities and consistently integrated into real-time collision assessment pipelines.

Recent research has increasingly focused on advanced braking control strategies that explicitly account for tire–road interactions and varying adhesion conditions. In particular, approaches based on optimal tire slip regulation using robust control techniques, such as H_∞ control, have been proposed to maximize braking performance under uncertain road conditions [8–11]. These methods aim to maintain the slip ratio near its optimal value, thereby ensuring maximum longitudinal force and minimizing stopping distance. Such developments highlight that braking capability is not a fixed parameter but a dynamic quantity dependent on both control strategy and road conditions. This perspective is directly relevant to the present work, as the proposed PONR formulation inherently incorporates braking capability as an important factor in defining the boundary between avoidable and unavoidable collision states, making it compatible with modern optimal braking control frameworks.

This paper introduces the Point of No Return as a physically grounded indicator that captures the transition between avoidable and unavoidable collision states. To illustrate its applicability, a perception-driven framework based on monocular vision is developed, enabling the joint analysis of TTC and PONR from observable data. This study highlights the complementary roles of the two indicators and shows that PONR provides an earlier and more physically interpretable characterization of critical situations. In addition, a PONR margin is introduced to describe the continuous evolution of the safety reserve. The approach is demonstrated on real-world driving sequences, illustrating its relevance for collision risk assessment in ADAS.

2. Models and Methodology

Vision-based forward collision warning systems often rely on monocular cameras and geometric distance estimation methods based on pinhole projection models and vehicle image features [12]. Monocular vision approaches estimate inter-vehicle distance from bounding-box geometry using the pinhole camera model and object dimension assumptions [13]. Vehicle tracking can be formulated as a recursive estimation problem in which the bounding-box location of the object is represented as a state vector and updated over time using a Kalman filter [14]. The Kalman filter is widely used in object tracking applications, where it predicts the next state of a detected object and updates it using new measurements obtained from object detectors [15]. Taylor and others in [16] present a Kalman-filter-based object tracking method that uses colour segmentation and the centre of the detected bounding box to estimate and predict an object's position while reducing processing time through cropped search windows.

Distance estimation from monocular images can be performed by exploiting the geometric relationship between the physical size of an object and its projected size in the image plane. Assuming a pinhole camera model, the distance to the object can be computed from the focal length and size of the detected bounding box in pixels [17,18]. Monocular distance estimation often relies on geometric relationships between the real dimensions of an object and its projected size in the image plane according to the pinhole camera model. However, width-based and height-based estimates may exhibit different sensitivity to perspective effects, camera pitch, and detection noise. Therefore, multiple scale cues can be fused to obtain a more robust distance estimate. Differential monocular object distance estimation method estimates object distance by combining different scale cues derived from bounding-box measurements over time, showing that bounding-box size information can be fused to improve monocular ranging accuracy [19].

Concepts related to collision inevitability have been studied in several contexts, including minimum safe distance models, braking distance analysis, and automatic emergency braking systems. These approaches rely on the relationship between vehicle speed, reaction

time, and braking capability to determine the critical distance beyond which collision avoidance becomes impossible [20,21].

According to [22], the time-to-collision metric represents the time remaining until two road users would collide, assuming constant velocities and unchanged trajectories, and is widely used as a surrogate indicator of collision risk in traffic safety analysis. In most forward collision warning (FCW) and AEB systems, the TTC metric is computed from the relative distance and velocity between the ego and lead vehicle and compared with predefined thresholds to determine the timing of driver warnings or braking interventions [23–25].

Traditional ADAS safety systems typically rely on the time-to-collision metric to trigger warnings when the estimated collision time falls below a predefined threshold. However, TTC assumes constant velocities and does not explicitly account for braking capability or reaction constraints, which motivates the introduction of alternative decision metrics such as the point of no return.

Therefore, modern safety systems incorporate additional metrics related to critical braking distance. The PONR, or a similar concept, is mentioned in [26–28]. Beyond this point, all physically achievable control actions inevitably lead to impact.

The steps for modelling and analysing the PONR importance in this paper are as follows:

- A formal monocular vision-based definition of PONR is introduced for longitudinal vehicle conflicts, where PONR is defined as the first instant at which the estimated inter-vehicle distance becomes smaller than the critical braking distance required for collision avoidance.
- A dashcam-oriented monocular distance estimation framework is developed by combining two complementary cues: object-scale estimation from the bounding-box width and height and ground-contact distance estimation from the lower edge of the bounding box, camera height mounting, and camera pitch.
- A unified estimation chain is proposed for real video analysis: vehicle detection/tracking–distance estimation–relative-speed estimation–TTC computation–PONR detection.
- The framework is formulated for rear-end conflicts, allowing distinct treatment of relative motion and effective deceleration in same-direction scenarios.
- PONR is compared conceptually and computationally with TTC, highlighting that TTC is a kinematic warning metric, whereas PONR represents a physically interpretable avoidability boundary.
- An additional interpretable indicator is introduced for analysis and visualization, the PONR margin, defined as the difference between the current distance and the critical braking distance.

Problem Definition

The present study addresses the estimation of the PONR in longitudinal vehicle conflict scenarios using a monocular dashcam. Rear-end collisions represent one of the most frequent crash types, accounting for nearly 30% of all traffic accidents [29]. This representative conflict configuration, in which the target vehicle travels in the same direction as the ego vehicle, is considered.

The main goal is to estimate, from image sequences alone and under known ego vehicle kinematic conditions, the distance to the target vehicle, the relative longitudinal speed, the TTC, and finally the PONR boundary.

Unlike conventional video-based collision warning approaches that rely primarily on TTC or distance thresholds, the proposed framework seeks to determine the last spatiotem-

poral state from which the collision can still be avoided by longitudinal braking. In this sense, PONR is treated as a physically interpretable decision boundary rather than a purely kinematic warning indicator.

The complete processing chain consists of the following:

- Vehicle detection in the image plane;
- Bounding-box tracking;
- Monocular distance estimation;
- Relative-speed estimation;
- TTC computation;
- PONR assessment.

The dashcam is modelled as a monocular pinhole camera with an intrinsic matrix defined in [30,31] with relation (1):

$$K = \begin{bmatrix} f_x & 0 & c_x \\ 0 & f_y & c_y \\ 0 & 0 & 1 \end{bmatrix}, \tag{1}$$

where f_x and f_y denote the focal lengths expressed in pixels, while c_x and c_y denote the coordinates of the principal point. For FullHD imagery (1920×1080), a practical approximation is as follows:

$$c_x \approx 960, c_y \approx 540, \tag{2}$$

In the present framework, the camera is assumed to be mounted at height h_{cam} above the road surface and tilted downward by a pitch angle θ. The pitch angle is defined as positive when the camera's optical axis is oriented toward the road surface.

In object detection tasks, objects are typically localized using rectangular bounding boxes that encode the spatial extent of the object in the image plane. A bounding box can be represented either by the coordinates of its upper-left and lower-right corners or by the centre coordinates together with the width and height of the rectangle [32,33]. In each frame k, the target vehicle is represented by a rectangular bounding box:

$$B_k = [x_k,\ y_k,\ w_k,\ h_k], \tag{3}$$

where x_k and y_k denote the top-left image coordinates, while w_k and h_k are the bounding-box width and height in pixels.

Vehicle detection is performed frame by frame using a YOLO-based detector (ref. [34]) constrained to road-relevant vehicle classes such as cars, trucks, buses, and motorcycles. Since raw frame-wise detections are subject to jitter, temporary misses, and shape fluctuations, the bounding box is temporally stabilized through a linear Kalman tracking formulation. The tracking state is defined as

$$X_k = \begin{bmatrix} c_{x,k} & c_{y,k} & w_k & h_k & \dot{c}_{x,k} & \dot{c}_{y,k} & \dot{w}_k & \dot{h}_k \end{bmatrix}^T, \tag{4}$$

where $c_{x,k}$ and $c_{y,k}$ are the center coordinates of the box, and $\dot{c}_{x,k}$, $\dot{c}_{y,k}$, $\dot{w}_k$, and $\dot{h}_k$ are the corresponding discrete-time rates.

Assuming constant velocity over one sampling interval Δt, the prediction model becomes

$$X_{k|k-1} = F X_{k-1|k-1}, \tag{5}$$

with transition matrix

$$F = \begin{bmatrix} 1 & 0 & 0 & 0 & \Delta t & 0 & 0 & 0 \\ 0 & 1 & 0 & 0 & 0 & \Delta t & 0 & 0 \\ 0 & 0 & 1 & 0 & 0 & 0 & \Delta t & 0 \\ 0 & 0 & 0 & 1 & 0 & 0 & 0 & \Delta t \\ 0 & 0 & 0 & 0 & 1 & 0 & 0 & 0 \\ 0 & 0 & 0 & 0 & 0 & 1 & 0 & 0 \\ 0 & 0 & 0 & 0 & 0 & 0 & 1 & 0 \\ 0 & 0 & 0 & 0 & 0 & 0 & 0 & 1 \end{bmatrix} \tag{6}$$

The detector measurement vector is

$$z_k = \begin{bmatrix} c_{x,k} & c_{y,k} & w_k & h_k \end{bmatrix}^T, \tag{7}$$

and the observation equation is given by

$$z_k = HX_k + v_k, \tag{8}$$

where

$$H = \begin{bmatrix} 1 & 0 & 0 & 0 & 0 & 0 & 0 & 0 \\ 0 & 1 & 0 & 0 & 0 & 0 & 0 & 0 \\ 0 & 0 & 1 & 0 & 0 & 0 & 0 & 0 \\ 0 & 0 & 0 & 1 & 0 & 0 & 0 & 0 \end{bmatrix} \tag{9}$$

The standard Kalman update is then applied through

$$K_k = P_{k|k-1}H^T\left(HP_{k|k-1}H^T + R\right)^{-1}, \tag{10}$$

$$X_{k|k} = X_{k|k-1} + K_k\left(z_k - HX_{k|k-1}\right), \tag{11}$$

$$P_{k|k} = (I - K_kH)P_{k|k-1}. \tag{12}$$

This tracking stage reduces the influence of frame-to-frame detection variability and enables short-duration target continuity when one or more detector outputs are temporarily missing.

The process noise covariance matrix Q is defined as a diagonal matrix:

$$Q = \begin{bmatrix} q_Z & 0 \\ 0 & q_V \end{bmatrix}, \tag{13}$$

where q_Z and q_V represent the uncertainty associated with the distance and relative velocity states, respectively. The measurement noise covariance matrix R is defined as

$$R = r_Z, \tag{14}$$

since only the distance is directly measured, while the relative velocity is estimated through the state model. The values of these parameters were determined through empirical tuning, considering the noise characteristics of the monocular distance estimation and the need to balance filtering smoothness with responsiveness to dynamic changes.

In paper [18], the authors estimate the distance to an object using a known object width and focal length, applying triangle similarity derived from the pinhole camera model. The method detects an object in the image and computes distance using the observed bounding-box size and the camera's focal length. Monocular distance estimation commonly relies on camera intrinsic parameters, focal length, and image measurements to infer object distance [35].

The current model estimates the first distance from the apparent dimensions of the detected bounding box. Let W_{real} and H_{real} denote the approximate real-world width and height of the target vehicle; assuming a calibrated pinhole projection, the distance can be estimated from the box width as

$$Z_W(k) = \frac{f_x W_{real}}{w_k}, \tag{15}$$

and from the box height as

$$Z_H(k) = \frac{f_y H_{real}}{h_k}. \tag{16}$$

Within the proposed methodology, the vehicle's dimensions, W_{real} and H_{real}, are not fixed a priori but are provided by the user for each individual case, depending on the type of vehicle observed in the video sequence. Thus, the model does not assume a single vehicle class but allows direct adaptation to the specific context (e.g., passenger car, truck, bus), significantly reducing the error associated with variability in real vehicle dimensions.

In addition, the YOLO-based detector used in this study already provides vehicle class differentiation (e.g., car, truck, bus), which enables the use of class-specific nominal dimensions. As a natural extension, the framework can be further enhanced by incorporating fine-grained vehicle recognition, e.g., make and model identification, allowing the automatic assignment of manufacturer-based dimensions and thus reducing the uncertainty in monocular distance estimation.

Since width-based and height-based estimates may exhibit different sensitivity to image perspective, pitch, and detection noise, the two are fused into a single scale-based estimate

$$Z_{bbox}(k) = \alpha Z_W(k) + (1 - \alpha) Z_H(k), \tag{17}$$

where $\alpha \in [0, 1]$ is a weighting factor. In practical automotive dashcam use, α is typically chosen in the range of 0.5 to 0.7, thereby assigning slightly greater weight to the width estimate when lateral contour preservation is more reliable than vertical contour completeness. The weighting factor reflects the relative reliability of different geometric cues used for distance estimation, consistent with prior work showing that distance can be decomposed into multiple complementary geometric factors (e.g., physical and projected dimensions) to improve robustness [36]. No fixed value of α is universally defined in the literature, as it depends on scene geometry and detection reliability; therefore, it is treated as a tunable parameter. This type of empirical weighting is common in monocular ranging and multi-cue fusion systems in ADAS. The parameters W_{real} and H_{real} correspond to nominal dimensions of the target vehicle class.

In addition to the scale-based distance, a second estimate is derived from the lower edge of the bounding box, which approximates the road-contact region of the target vehicle. This geometric cue is especially useful at short range, where bounding-box width and height may become unstable because of strong perspective, clipping, or detection saturation.

Let the vertical coordinate of the lower edge of the bounding box be

$$y_{b,k} = y_k + h_k. \tag{18}$$

The corresponding image-plane ray angle relative to the optical axis is

$$\phi_k = \arctan\left(\frac{y_{b,k} - c_y}{f_y}\right). \tag{19}$$

Assuming that the observed lower edge lies on the road plane and that the camera is mounted at height h_{cam} with downward pitch angle θ, the distance from the camera to the target along the road plane is estimated as

$$Z_{ground}(k) = \frac{h_{cam}}{\tan(\theta + \phi_k)}. \tag{20}$$

The ground-contact point of the object is obtained by projecting the lower edge of the bounding box into the scene; using the camera's height and pitch angle, the longitudinal distance Z is computed via simple geometric relations, as shown in Figure 3.

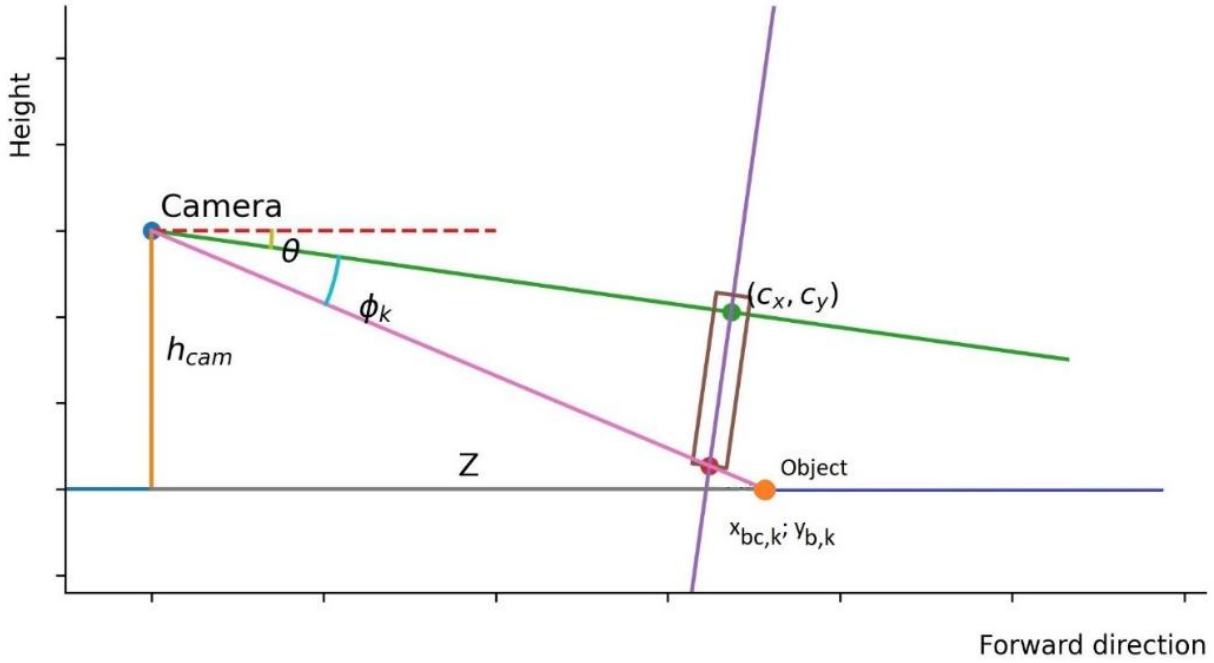

Figure 3. Ground-contact distance estimation from the bounding box's lower edge.

The camera pitch angle θ is defined as the angle between the optical axis of the camera and the horizontal plane of the road. This formulation makes the distance estimate explicitly dependent on the dashcam installation geometry. In practical use, typical mounting parameters are $h_{cam} \approx 1.2$ to 1.4 m and $\theta \approx 2^\circ$ to 5°.

The ground-contact estimate is highly sensitive to pitch and principal-point errors but is often more physically consistent at close range than a pure scale-based estimate.

The final raw distance estimate is obtained by combining the scale-based and ground-contact estimates:

$$Z_{raw}(k) = (1 - \beta) Z_{bbox}(k) + \beta Z_{ground}(k), \tag{21}$$

where $\beta \in [0, 1]$ controls the contribution of the ground-contact geometric cue. A practical range for dashcam analysis is $\beta \approx 0.2$ to 0.5. For example, $\beta = 0.35$ gives a moderate influence on the ground estimate while preserving consistency against pitch uncertainty.

To suppress outliers and frame-wise jitter, the raw distance signal is further filtered using median smoothing and/or a low-order Kalman or IIR scheme. The filtered output is denoted by $Z(k)$ and represents the final inter-vehicle distance used for subsequent kinematic computations.

The relative longitudinal speed is computed from the temporal derivative of the filtered distance signal. In continuous form,

$$v_{rel}(t) = -\frac{dZ}{dt}. \tag{22}$$

The negative sign ensures that positive relative speed corresponds to decreasing distance, i.e., to an approaching target.

In discrete form, the raw relative speed is approximated by

$$v_{rel}[k] = -\frac{Z[k] - Z[k-1]}{\Delta t}. \tag{23}$$

Because finite-difference differentiation amplifies noise, a filtered version is used in the following implementation:

$$v_{rel,f}[k] = \lambda v_{rel,f}[k-1] + (1-\lambda) v_{rel}[k], \tag{24}$$

where λ is a smoothing parameter. Typical values lie between 0.7 and 0.9. The filtered signal $v_{rel,f}$ is the one retained for TTC and PONR estimation.

Hayward defined TTC as the time remaining until two vehicles would collide if they continue with unchanged speeds and trajectories [22]. The time to collision is computed whenever the target is approaching, i.e., for $v_{rel} > 0$. It is defined as

$$TTC(k) = \frac{Z(k)}{v_{rel}(k)}. \tag{25}$$

If $v_{rel} \leq 0$, the target is not approaching in the collision sense, and TTC is treated as undefined or effectively infinite.

Although TTC is widely used as a collision-risk metric, it remains purely kinematic and does not explicitly account for reaction delay or available braking capability. This limitation motivates the introduction of PONR as the primary decision metric of the present study.

The Point of No Return is defined as the first instant at which the current inter-vehicle distance becomes smaller than the minimum distance required for collision avoidance through longitudinal braking. Formally, the PONR condition is

$$Z(k) \leq D_{crit}(k), \tag{26}$$

where D_{crit} is the critical braking distance.

In [37], the critical distance required to avoid collision can be expressed as the sum of the reaction distance and braking distance, commonly formulated as $D_{crit} = vt_{react} + \frac{v^2}{2a}$, which is widely used in vehicle safety and stopping sight distance models. Also, in [38], the authors use a similar formula, and the perception-reaction time ranged from 0.48 to 2.01 s, with a total weighted average of 1.21 s.

In our model, for same-direction motion, the effective relative deceleration is

$$arel(t) = \frac{dv_{rel}(t)}{dt}. \tag{27}$$

The relative acceleration $a_{rel}(k)$ is computed as the discrete-time derivative of the relative velocity and filtered to reduce noise introduced by differentiation.

The discrete-time index k corresponds to the frame index of the video sequence, with the associated time defined as $t_k = k\Delta t$, where Δt is the sampling interval determined by the video frame rate. Therefore, all kinematic quantities, including the relative acceleration $a_{rel}(k)$, are computed in discrete time based on frame-to-frame measurements. The continuous-time notation $a_{rel}(t)$ is used for conceptual clarity.

Thus, the critical distance is then written as

$$D_{crit}(k) = v_{rel}(k) t_{react} + \frac{v_{rel}^2(k)}{2a_{rel(k)}} + \tau, \tag{28}$$

where t_{react} denotes the total reaction time, including detection, processing, and actuation delay, and τ is a fixed safety offset. A reduction in the reaction time decreases the critical distance D_{crit}, which shifts the Point of No Return closer to the obstacle and delays its occurrence in time. Consequently, the TTC value at PONR also decreases. The τ term represents a safety buffer that compensates for uncertainties inherent to monocular distance estimation, as well as unmodeled vehicle dynamics and real-world braking limitations. Near-zero values of relative deceleration may lead to numerical instability in the braking term of the critical distance formulation. In the proposed implementation, this issue is addressed by introducing a lower bound for the effective relative deceleration. Specifically, the deceleration term is constrained as $a_{rel,eff} = \max(\mid a_{rel} \mid, 0.5)$, ensuring that the denominator in the braking term remains well-defined and preventing unrealistic growth of the expression $\frac{v_{rel}^2}{2a_{rel}}$. This approach ensures numerical stability while also reflecting a physically meaningful assumption, as extremely low deceleration values correspond to situations where effective braking is not available. To avoid near-singular growth of the braking term at very low deceleration values, a lower bound of 0.5 m/s^2 was adopted for the effective relative deceleration, ensuring numerical stability while conservatively shifting the PONR boundary earlier through an increase in the critical distance.

In the current formulation, the effect of braking capability is implicitly included through the relative deceleration term used in the computation of the critical distance D_{crit}, which underlies the determination of PONR. This term can be interpreted as an effective deceleration that aggregates both the braking performance of the following vehicle and the tire–road interaction conditions. Regarding road conditions, these are not explicitly modelled through a variable friction coefficient but are indirectly reflected through the deceleration values considered in the analysis. This choice was made to maintain the applicability of the methodological framework under real-world conditions, where robust online estimation of the adhesion coefficient remains challenging.

To improve interpretability, a supplementary indicator is introduced, and the PONR margin is defined as

$$M_{PONR}(k) = Z(k) - D_{crit}(k). \tag{29}$$

If $M_{PONR} > 0$, braking-based collision avoidance remains feasible. If $M_{PONR} = 0$, the system is exactly at the PONR boundary. If $M_{PONR} < 0$, the conflict has entered a beyond-PONR region.

An important practical aspect of the framework concerns the interpretation of the initial and final distance estimates. The initial distance is not necessarily the distance in the very first frame of the video. Instead, it is defined as the first valid distance estimate obtained after successful target acquisition. In other words, if the detector does not yet provide a stable bounding box in the early frames, the analysis starts only when the target has been reliably detected and associated. Therefore, the initial distance is

$$Z_{init} = Z(k_0), \tag{30}$$

where k_0 is the first valid frame used in the analysis.

Similarly, the final distance is defined as the last valid estimate retained by the processing chain:

$$Z_{final} = Z\left(k_f\right), \tag{31}$$

where k_f is the last accepted frame. If the last frame contains a valid detector output, then Z_{final} is detector-supported. If the detector output is temporarily unavailable and the target is maintained through short-horizon tracking, then the final distance should be interpreted as tracker-supported rather than directly detector-measured.

From a reporting perspective, it is therefore useful to distinguish between the following:

- The last distance based on a valid YOLO detection.
- The last distance propagated by the tracker only.
- The final filtered distance displayed by the framework.
- This distinction is essential when interpreting close-range end-of-sequence behaviour.

The proposed methodology transforms monocular dashcam imagery into a physically grounded collision-avoidance assessment chain. A detected and tracked vehicle bounding box is first converted into distance using scale-based and ground-contact geometric models. The estimated distance is then filtered and differentiated to obtain relative speed, from which TTC and the critical braking distance are computed. Finally, the PONR boundary is identified as the first instant when the available inter-vehicle distance becomes insufficient for collision avoidance by braking.

By construction, TTC remains a descriptive kinematic indicator, whereas PONR acts as an avoidability-based decision boundary. This distinction constitutes the methodological core of the present framework.

3. Experimental Setup

The objective of the experimental evaluation is to validate the relevance of the PONR indicator, in comparison with TTC, for describing and anticipating critical collision scenarios using quantities well estimated from monocular video data. The experiments focus on longitudinal vehicle conflicts and aim to demonstrate that the proposed framework can reliably estimate distance, relative speed, and the PONR boundary using only bounding-box observations obtained from dashcam video.

The experimental framework was implemented in MATLAB 2025a, using a custom graphical interface that integrates YOLO-based vehicle detection, Kalman-based bounding-box tracking, monocular distance estimation, and TTC and PONR computation.

The interface enables both video-based experiments and synthetic scenario analysis, allowing parameter sensitivity studies for reaction time, braking capability, and camera geometry.

The experiments assume a typical automotive dashcam installation mounted inside the ego vehicle. The camera records FullHD video with a resolution of 1920×1080 pixels at a frame rate of 30 fps. The camera is mounted approximately at the windshield centre with a height relative to the road surface of h_{cam} = 1.42 m. The optical axis is assumed to be slightly inclined downward with a pitch angle $\theta = 2^{\circ}$. The intrinsic parameters used in the experiments correspond to effective central-ROI focal lengths for a wide-angle dashcam.

The camera field of view angle is determined geometrically from the ratio between the visible scene width and the distance to the object according to the following relation: The half-angle satisfies $\tan(\alpha/2) = \frac{D/2}{L}$, as shown in Figure 4. Assuming a pinhole camera model and square pixels, the focal length in pixels is computed from the horizontal field of view as $f_x = \frac{W}{2\tan\left(\frac{\alpha}{2}\right)}$, while $f_y \approx f_x$. The focal length was experimentally estimated using a geometric calibration setup, resulting in $f_x \approx f_y \approx 856$ px, consistent with the horizontal field of view derived from the measured baseline and camera distance. The principal point is approximated as the centre of the image: $c_x = 960$, $c_y = 540$.

Vehicle detection is performed using a YOLO-based object detector trained in road-vehicle categories. In each frame, the detector provides a set of bounding boxes with associated confidence scores, as shown in Figure 5. Only detections belonging to vehicle classes, i.e., cars, trucks, buses, or motorcycles, and those located within a predefined road-oriented region of interest are considered.

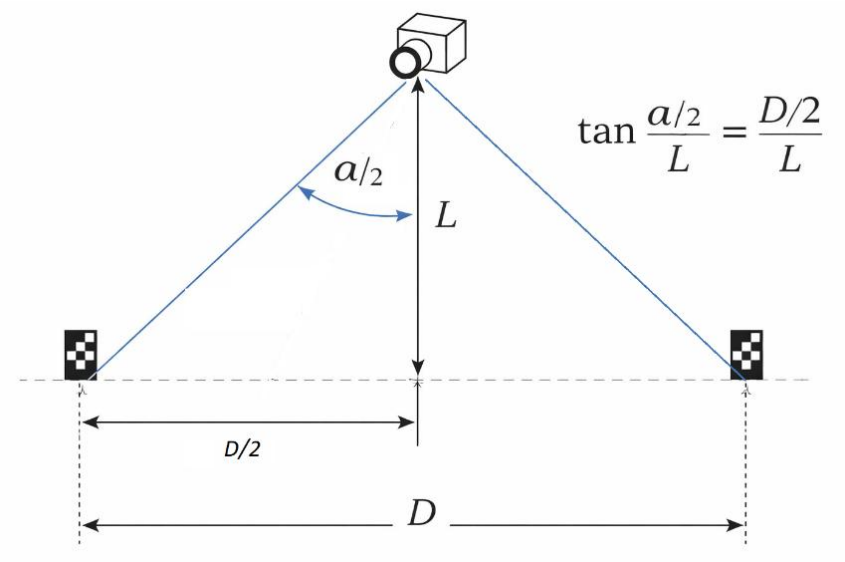

Figure 4. Camera angle of view calibration.

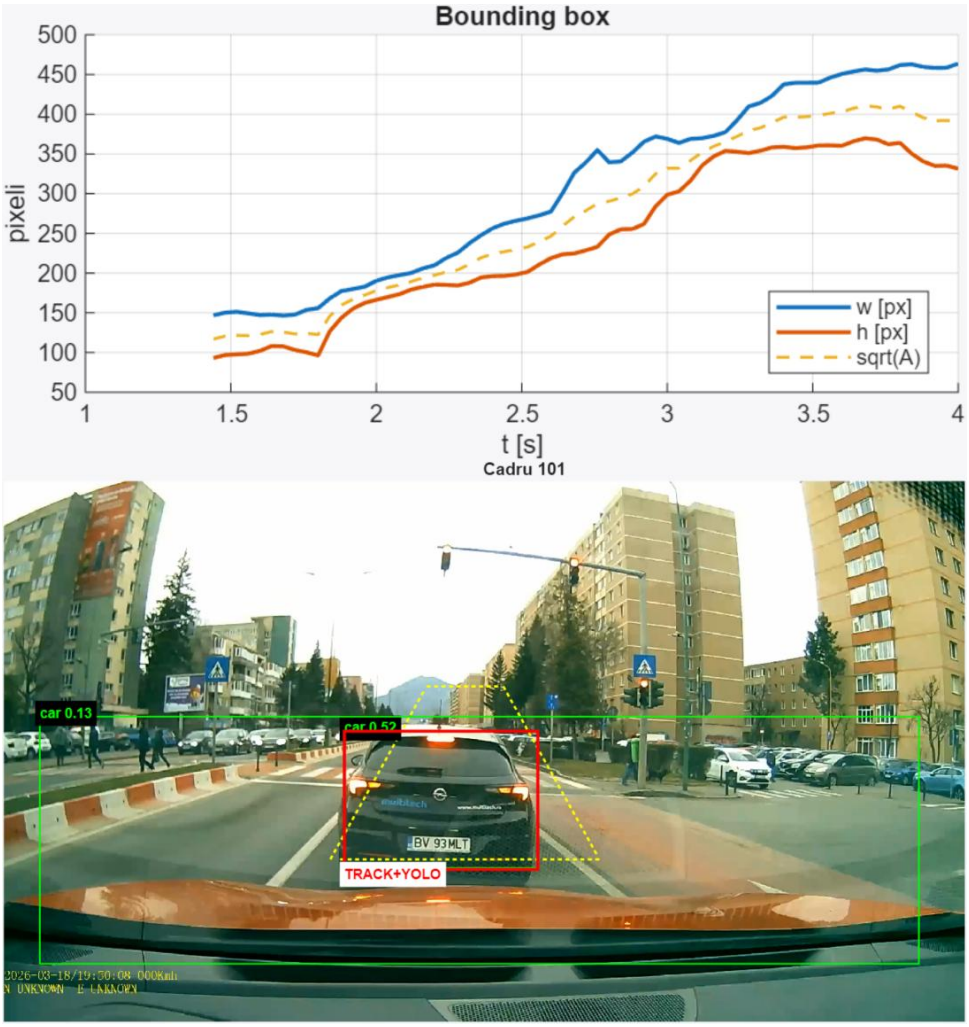

Figure 5. Example of temporal evolution of bounding-box dimensions during target approach (**up**) and vehicle YOLO detection during analysis (**down**).

https://doi.org/10.3390/app16083869

The target vehicle is selected as the detection whose centre is closest to the image centre along the road axis and whose bounding box satisfies basic size and confidence thresholds.

To ensure temporal consistency, detections are passed to a Kalman-based tracker, which performs frame-to-frame association and bounding-box smoothing. The tracker maintains a state vector containing the bounding-box centre coordinates, width, height, and their temporal derivatives.

The tracker fulfils three main functions:

- Smoothing detection jitter;
- Maintaining target identity across frames;
- Propagating the bounding box during brief detector dropouts.

The bounding box used in the distance estimation stage is therefore the filtered output of the detection–tracking chain.

For each frame, the inter-vehicle distance is estimated, as shown in Figure 6, using the fusion method described in Section 2. Two complementary distance estimates are computed: scale-based distance and ground-contact distance. The two estimates are fused in Equation (21) with $\alpha = 0.6$ and $\beta = 0.35$. These values are not arbitrary, but were selected empirically based on preliminary tests, with the objective of achieving a balance between stability and accuracy. In particular, the value $\alpha = 0.6$ assigns a slightly higher weight to the width-based estimation of the bounding box, which proved to be more stable under real traffic conditions, while the height-based estimation is more sensitive to perspective variations and occlusions. Similarly, $\beta = 0.35$ introduces a moderate contribution of the ground-contact-based estimation, which is more robust at short distances but more sensitive to calibration errors. To assess the influence of these parameters, a sensitivity analysis was conducted by varying α and β within realistic ranges ($\alpha \in [0.4, 0.8]$, $\beta \in [0.2, 0.5]$), as shown in Table 1.

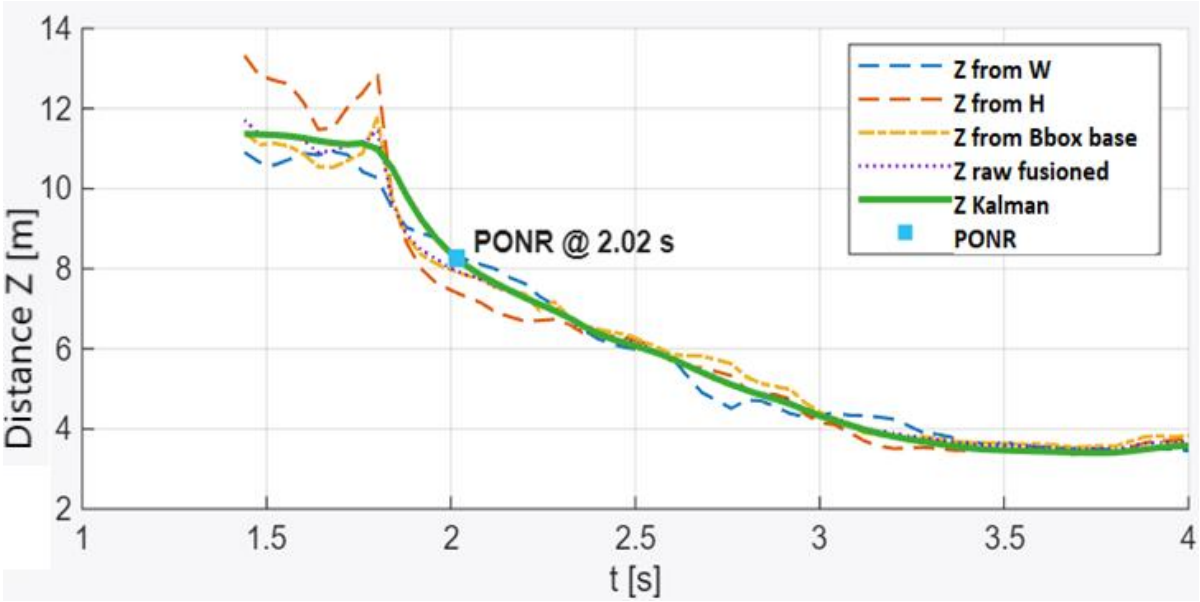

Figure 6. Estimated distance evolution and PONR identification (extracted from real test).

Table 1. Sensitivity of distance estimation to fusion weights.

α	β	Observed Effect
0.4	0.2	Increased sensitivity to bounding-box height noise; less stable distance estimation
0.6	0.35	Balanced performance; stable estimation across medium range (baseline setting)
0.8	0.5	Higher influence of ground geometry; improved short-range accuracy but increased sensitivity to calibration errors

The analysis shows that α primarily affects robustness in detecting noise and perspective distortions, while β influences the trade-off between geometric consistency and sensitivity to camera calibration parameters. Importantly, variations in these parameters mainly affect the absolute distance scale, while the temporal evolution of distance and thus the estimation of relative speed remains comparatively stable due to filtering. As a result, the impact on TTC is moderate, and the effect on PONR detection is limited. These results indicate that the proposed fusion scheme is robust within a reasonable parameter range.

Finally, a temporal smoothing filter is applied to obtain the filtered distance $Z(k)$. This distance represents the longitudinal separation between the ego vehicle and the detected target vehicle.

To validate the distance estimation approach, the actual final distance between the vehicles was measured and compared with the value obtained from the proposed framework. The resulting error was below 10%, indicating an acceptable level of accuracy for the subsequent analysis. This value refers to the error evaluated at the final stage of the analyzed sequences, when the vehicles come to a stop. In this case, the reference distance was obtained through direct physical measurement and compared with the final distance estimated by the proposed method. Therefore, the reported error represents a final-frame validation against a physically measured reference, rather than an average or maximum error over all frames. Only the cases in which technical conditions allowed a safe physical measurement of the distance between vehicles after they had come to a complete stop were considered in the analysis.

The relative longitudinal speed between the two vehicles is computed from the discrete derivative of the estimated distance relation (22), Figure 7 top view, to reduce numerical noise caused by frame-to-frame measurement variations, the resulting signal is filtered using a first-order exponential smoothing filter using relation (24), with the coefficient $\lambda = 0.8$. The filtered relative speed is then used to compute the time to collision, TTC, as shown in the bottom of Figure 7.

The Point of No Return represents a decision threshold, whereas the minimum TTC serves as an indicator of interaction severity and is a reactive indicator reflecting how critical a situation has become, and PONR is a predictive threshold indicating when collision avoidance is no longer possible. The Point of No Return is consistently reached before the minimum TTC, confirming that the loss of collision avoidance capability occurs prior to the most critical interaction state. TTC_{min} values below one second indicate a highly critical situation close to collision, and values between 1 and 2 s correspond to elevated risk, while values above 3 s generally reflect relatively safe interaction conditions. If the relative speed is negative or zero, the vehicles are diverging, and TTC is considered undefined for collision-risk evaluation.

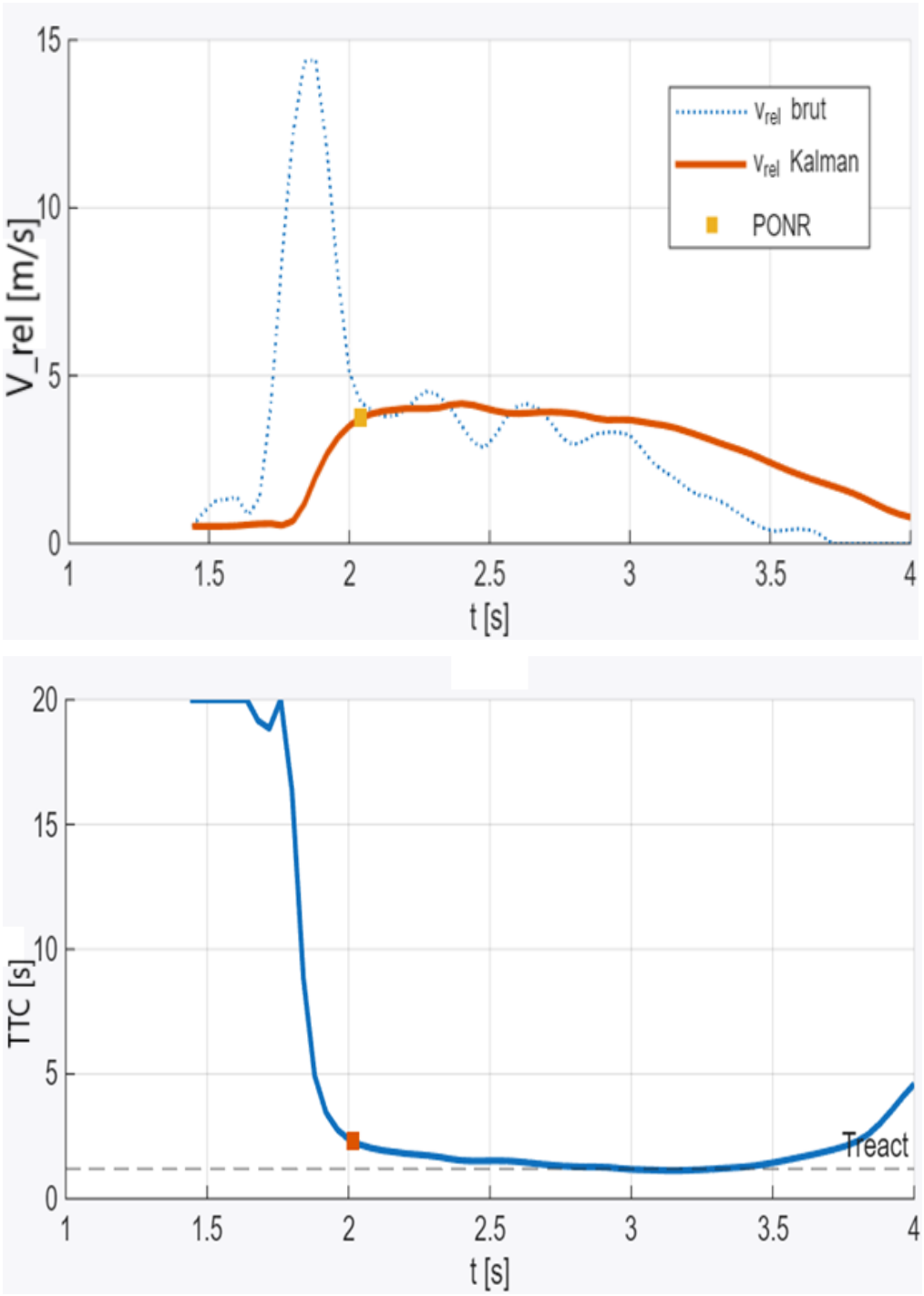

Figure 7. Raw and Kalman-filtered relative speed (**up**) and TTC evolution (**bottom**) (extracted from real test).

In the current implementation, the ego vehicle speed is assumed constant over one sampling interval and referenced to the initial simulation time, while object detection and tracking may start at a later instant. This temporal misalignment introduces a bias in the estimation of relative speed and derived quantities. The temporal misalignment between detection and ego vehicle speed is not a persistent issue across all analyzed sequences but rather a potential source of bias that may occur in certain situations, depending on the synchronization between video frames and vehicle motion. In the present study, the relative speed is estimated from the temporal evolution of the distance, which makes the method less dependent on explicit ego vehicle speed measurements. As a result, the impact

of such misalignment is limited and does not systematically affect all sequences but may introduce small variations in specific cases.

Therefore, a proper synchronization between the detection timestamp and the corresponding ego vehicle speed is required to ensure physically consistent results. The first-order analysis shows that TTC is inversely proportional to the square of the relative speed, making it highly sensitive to small errors in relative speed estimation, especially at low velocities. Similarly, the impact on PONR is indirect through its dependence on v_{rel} in the critical distance formulation. However, because PONR is dominated by the braking term and includes a safety margin, its sensitivity to small velocity perturbations is lower than that of TTC. Importantly, the introduced bias is systematic but bounded and does not affect the main conclusion of this study. The relative ordering between TTC and PONR remains unchanged, with PONR consistently identifying the transition to collision inevitability earlier than TTC-based thresholds.

In the current implementation, the ego vehicle speed is used as contextual information for scenario description and result interpretation, while TTC and PONR are computed exclusively from the estimated relative motion. The bias introduced by the assumption of constant ego vehicle speed and the temporal misalignment between detection and vehicle state can be approximated as $\Delta v_{rel} \approx a_{ego}\Delta t$. For typical acquisition rates of 30–10 fps, $\Delta t \approx 0.033$–0.10 s, and moderate ego vehicle accelerations/decelerations are $a_{ego} = 1$–2 m/s^2; the resulting error in relative speed remains limited to approximately 0.03–0.20 m/s.

For a representative scenario with $v_{rel} = 5$–6 m/s and $Z = 15$–20 m, this corresponds to a TTC variation of approximately 0.01–0.16 s. The impact on PONR is smaller, as it depends not only on the estimated relative speed but also on braking dynamics, reaction time, and safety margin. Therefore, while this bias exists, it remains bounded and does not affect the main conclusion regarding the earlier and more robust behaviour of the PONR threshold compared to TTC.

A non-zero residual relative speed may still appear at the end of the manoeuvre because the relative speed is not directly measured but estimated from the temporal derivative of the monocular distance signal. Small fluctuations in the detected bounding box and filtering inertia may therefore generate residual non-zero velocity estimates even when both vehicles are stationary.

The PONR calculation requires additional parameters related to vehicle dynamics and driver/system reaction. The following values are adopted as representative for passenger vehicles: reaction time: $t_{react} = 1.2$ s, according to [38,39]; maximum ego deceleration: $a_{ego} =$ between 0 and 7.5 m/s^2; safety margin: $\tau = 3$ m. The critical braking distance is then computed using (26). The PONR moment is identified as the first frame satisfying relation (24), as shown in Figure 8. Reaction time is the dominant parameter influencing D_{crit} and TTC_{PONR}, while the safety margin produces a consistent offset, both contributing to an earlier and more conservative identification of the PONR boundary.

The value of safety margin was not intended as a vehicle-specific constant but as a conservative buffer introduced to account for monocular distance-estimation uncertainty, filtering lag, and unmodeled braking limitations. In addition, we now explicitly state that effective deceleration is scenario-dependent and governs the braking term of the critical distance formulation, as shown in Equation (28). We added a sensitivity analysis in which reaction time, effective deceleration, and margin were varied over realistic ranges, as shown in Table 2. The results confirm the expected monotonic behaviour: Increasing reaction time or safety margin shifts the PONR boundary earlier and increases TTC at PONR, while increasing available deceleration delays the PONR boundary and reduces TTC at PONR. Importantly, although the absolute PONR location changes with parameter selection, the

main conclusion remains unchanged; PONR consistently identifies the loss of avoidability earlier than TTC-based criticality indicators. These clarifications and the new sensitivity study have been added to improve both the physical interpretability and robustness of the proposed framework.

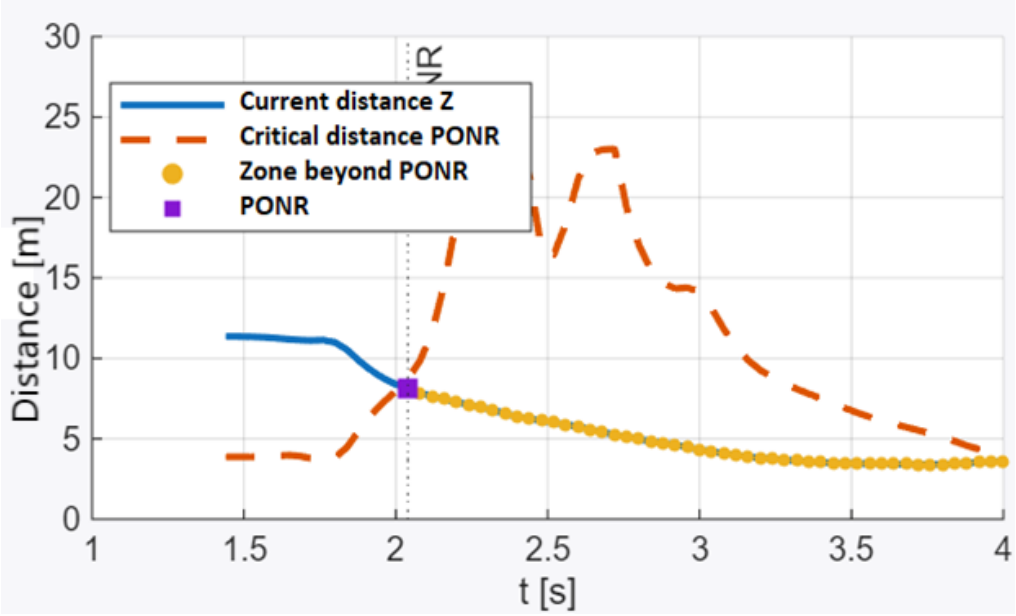

Figure 8. PONR determination from Z distance and D_{crit} (extracted from real test).

Table 2. Parametric influence on PONR boundary.

Parameter	Variation	Effect on D_{crit}	Effect on PONR Timing	Effect on TTC_{PONR}
t_{react}	Increase	Linear increase	Earlier	Increase
t_{react}	Decrease	Linear decrease	Later	Decrease
τ	Increase	Uniform additive shift	Earlier	Slight increase
τ	Decrease	Uniform reduction	Later	Slight decrease
a_{rel}	Increase	Nonlinear decrease ($\sim 1/a_{rel}$)	Later	Decrease
a_{rel}	Decrease	Nonlinear increase ($\sim 1/a_{rel}$)	Earlier	Increase

A reduction in effective deceleration, due to low adhesion conditions or reduced braking performance, leads to a clear increase in the critical braking distance and shifts the PONR boundary earlier. For the considered urban scenario ($v_{rel} = 6$ m/s), decreasing a_{rel} from 8 m/s^2 to 2 m/s^2 increases D_{crit} from 12.45 m to 19.20 m and raises TTC_{PONR} from 2.08 s to 3.20 s. This variation highlights that PONR is strongly dependent on braking capability, confirming its physical nature and its advantage over TTC, which does not explicitly account for this effect.

The experiments evaluate the following indicators:

- Estimated inter-vehicle distance $Z(t)$.
- Relative speed $v_{rel}(t)$.
- Time to collision $TTC(t)$.
- Critical braking distance $D_{crit}(t)$.
- PONR margin $M_{PONR}(t) = Z(t) - D_{crit}(t)$.

These metrics allow direct comparison between TTC-based warnings and PONR-based avoidability boundaries.

4. Results and Discussion

The proposed methodology was evaluated using a set of 24 real-world driving sequences acquired with a monocular onboard camera. The analyzed scenarios correspond to rear-end situations under same-direction traffic conditions, with varying ego vehicle speeds and different relative motion configurations.

For each run, object detection and tracking were performed using a YOLO-based framework, and the relative distance $Z(t)$ was estimated from bounding-box geometry. The relative speed was derived from the temporal variation in the estimated distance, followed by Kalman filtering.

The following key indicators were extracted for each sequence, minimum time to collision TTC_{min}, time to collision at the Point of No Return TTC_{PONR}, relative speed, and acceleration. Importantly, no external sensors (e.g., radar, LiDAR, CAN, or GPS) were used, ensuring that all results are based exclusively on monocular visual perception.

Across the analyzed dataset, the minimum TTC values ranged between 0.7 s and 2.9 s, indicating situations varying from moderate to critical risk. In contrast, the TTC values corresponding to the Point of No Return were consistently higher, typically within the range of 2 s to 3.2 s for most scenarios, as shown in Figure 9. This behaviour reveals a fundamental distinction between the two indicators:

- TTC is a continuously decreasing metric that reflects the remaining time until collision under current conditions.
- PONR represents a discrete transition point, marking the onset of collision inevitability.

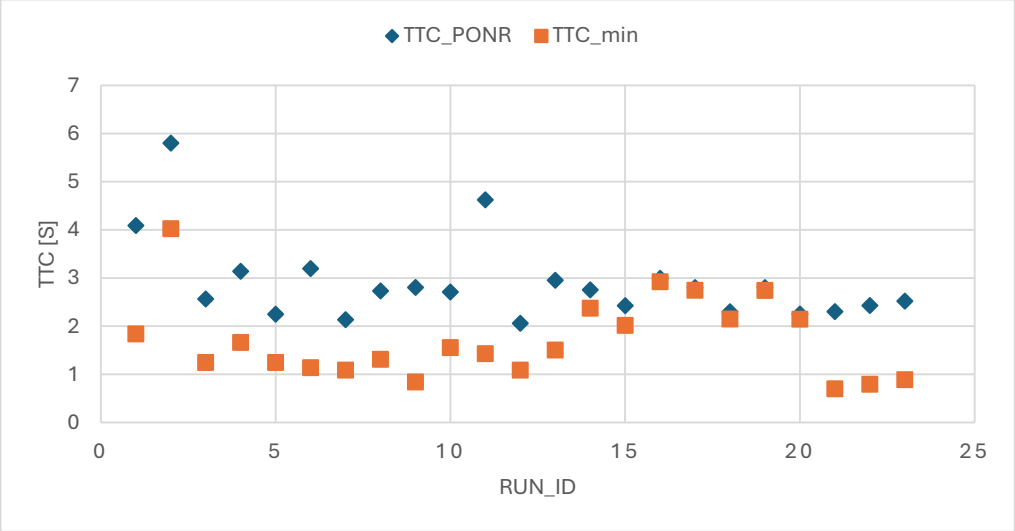

Figure 9. Comparison of the TTC value at the PONR and the minimum TTC across all experimental runs.

The experimental results clearly show that $TTC_{PONR} > TTC_{min}$ for most cases. This confirms that the transition to an unavoidable collision occurs significantly earlier than the moment when TTC reaches its minimum value.

The relatively higher values of TTC_{PONR} and TTC_{min} observed in Figure 9 may be attributed to the conservative parameter choices adopted in this study, including a reaction time of $t_{react} = 1.2$ s and a safety margin of 3 m. These parameters increase the estimated critical distance D_{crit} and shift the Point of No Return toward earlier stages of the interaction, which in turn leads to higher TTC values compared to those reported in studies based on more idealized or lower-margin assumptions.

Studies on rear-end scenarios indicate that TTC values around 0.5–1 s correspond to near-collision or unavoidable conditions, while practical AEB intervention thresholds are typically set between 1.25 and 2 s [40–42]. Furthermore, PONR-related thresholds, such

as the time-to-react (TTR) value of approximately 0.5 s with physical limits around 0.8 s reported in [43], define the latest feasible intervention point.

The results presented in Figure 9 are consistent with these findings. TTC_{min} is predominantly observed in the range of 0.7–2.9 s, reflecting interaction severity, while TTC at PONR is systematically higher, typically between 2 and 3.2 s. This separation confirms that TTC at PONR captures the last avoidable state, whereas TTC_{min} reflects the subsequent evolution toward the most critical interaction.

One of the most relevant findings is that the PONR consistently anticipates critical situations compared to classical TTC-based assessment. For example, in multiple scenarios, the difference between TTC_{PONR} and TTC_{min}, $\Delta TTC = TTC_{PONR} - TTC_{min}$, exceeds one second, as shown in Figure 10. From a safety perspective, this temporal margin is highly significant, as it represents additional time available for intervention (e.g., braking or evasive manoeuvres). Positive values indicate that PONR provides earlier identification of critical situations. This result suggests that TTC-based systems may react too late, particularly when relying on fixed TTC thresholds, whereas PONR identifies the last feasible moment for collision avoidance.

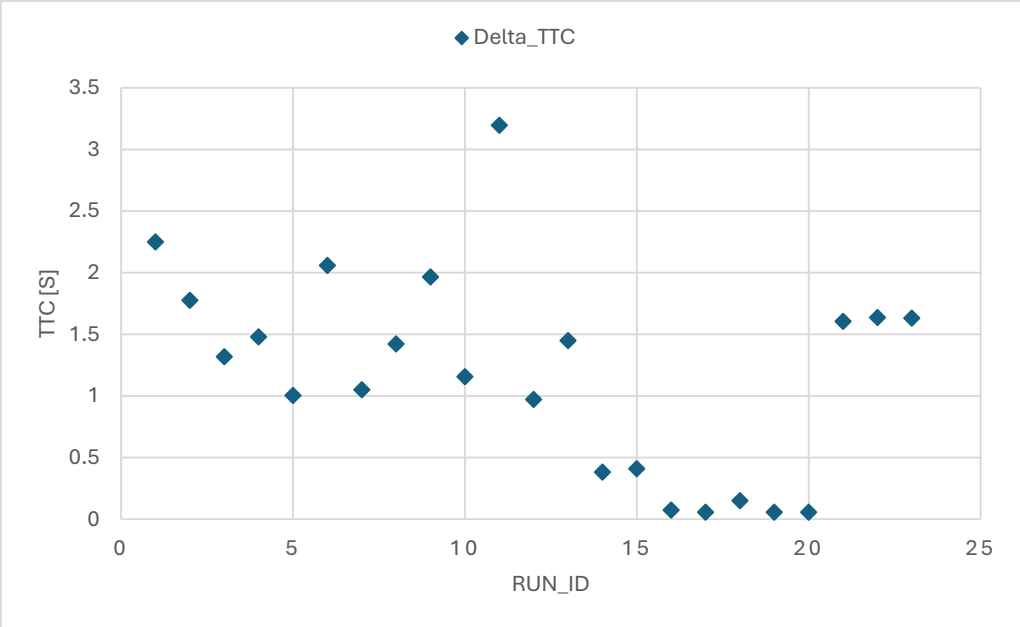

Figure 10. Difference between TTC at PONR and minimum TTC (ΔTTC) for all tested scenarios.

The experimental data show a strong dependency of TTC_{min} on relative speed. Higher relative velocities lead to significantly lower minimum TTC values, as expected from the definition. However, the PONR exhibits a different behaviour. While it is influenced by speed, it remains comparatively more stable across scenarios. Even in cases with high relative speeds (see $v_{rel} > 5$ m/s), the TTC_{PONR} values remain within a relatively narrow band, as shown in Figure 11.

The results show that the minimum TTC is more sensitive to relative speed variations, whereas the PONR threshold remains comparatively more stable, so it is more stable in tested conditions and a structurally meaningful indicator.

In scenarios with very low relative speeds and near-stationary or slowly approaching targets, the PONR occurs at significantly higher TTC values. This is physically consistent, as the system correctly identifies that collision risk is low and the transition to inevitability is either delayed or practically irrelevant. Unlike TTC, which may still fluctuate due to noise or estimation errors, the PONR does not generate misleading critical events in

such cases. This highlights its resistance to false alarms, an important requirement for ADAS applications.

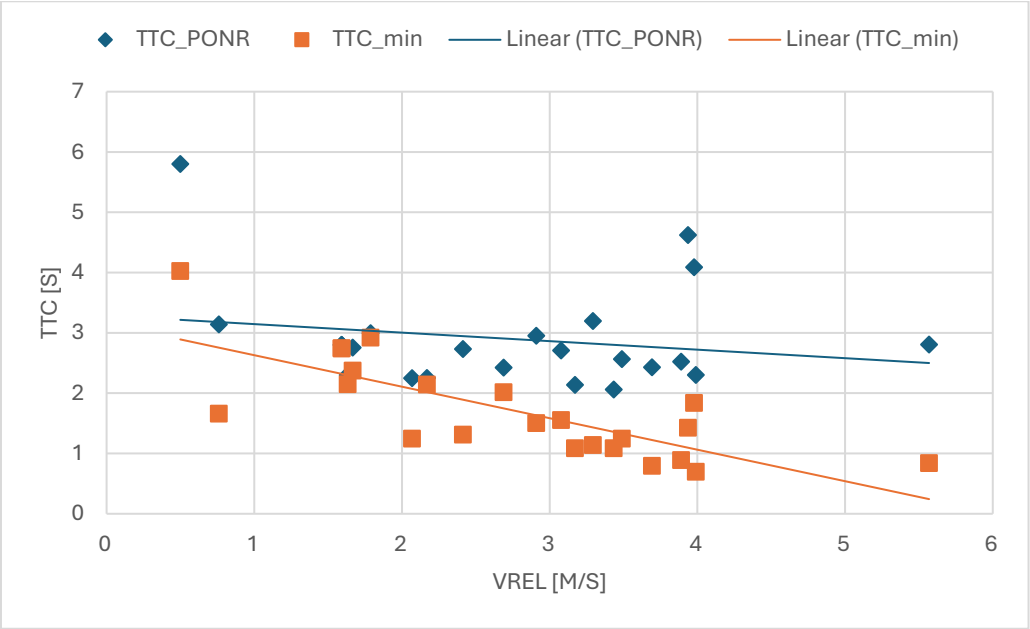

Figure 11. Relationship between mean relative speed and the two risk indicators, TTC_{PONR} and TTC_{min}.

For constant initial speed conditions, a gradual reduction in braking deceleration leads to a systematic increase in TTC_{PONR}, while TTC_{min} remains unchanged. This indicates that TTC_{PONR} is strongly dependent on the vehicle's braking capability, reflecting the shift of the last avoidable state, whereas TTC_{min} is primarily governed by the kinematic evolution of the scenario and does not capture variations in braking performance, as shown in Figure 12.

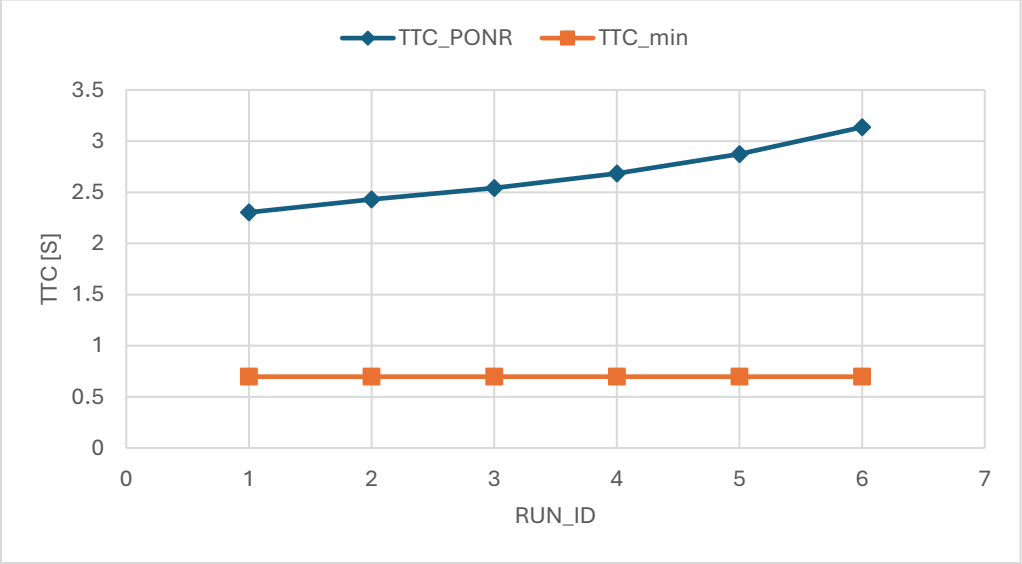

Figure 12. Influence of maximum deceleration on TTC_{PONR} and TTC_{min} for identical initial speed.

To interpret the braking capability used in the simulated PONR analysis, the user-defined ego deceleration a_{ego} was further expressed as an equivalent friction coefficient, $\mu_{eq} = a_{ego}/g$. This enabled the investigated scenarios to be associated with different effective road adhesion conditions, ranging from low-friction to high-friction surfaces. The

results showed that lower equivalent friction levels led to larger critical stopping distances and earlier PONR occurrence, confirming that PONR is sensitive to braking capability, unlike a fixed TTC threshold, as shown in Figure 13. Furthermore, modern ADAS systems do not rely on the target vehicle's absolute speed or deceleration, v_{obj} and a_{obj}, but instead operate primarily on relative kinematic quantities, reinforcing the validity of the proposed approach. This trend demonstrates that PONR inherently captures the effect of braking capability, expressed through μ_{eq}, whereas TTC alone remains insensitive to such variations, reinforcing the consistency and practical relevance of the proposed indicator.

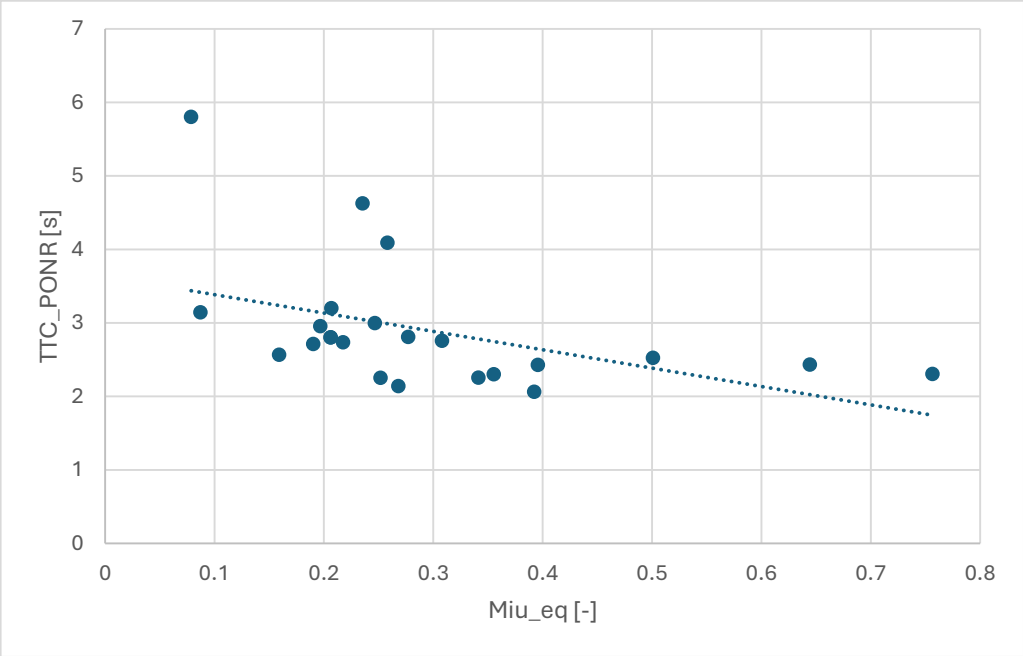

Figure 13. PONR time vs. equivalent friction coefficient.

Although PONR is theoretically derived using maximum braking capabilities, corresponding to high adhesion levels, μ ≈ 0.8–0.9, the experimental analysis employs an equivalent friction coefficient between μ ≈ 0.2 and 0.75 in most cases to reflect real-world effective deceleration conditions, where driver response, system limitations, and road variability prevent vehicles from consistently achieving ideal maximum braking performance. This also highlights the importance of real-time estimation of the road–tire friction coefficient, which would enable a more accurate and adaptive determination of PONR under varying driving conditions [42,44].

The PONR margin provides a continuous measure of safety reserve, capturing both the transition from avoidable to unavoidable collision states through its zero-crossing and the severity of the conflict through the magnitude of its negative values, thereby offering additional insight beyond the discrete identification of the PONR instant, as shown in Figure 14.

We emphasize that the objective of this study is the comparative analysis of two indicators, TTC and PONR, and the highlighting of the fundamental difference between a kinematic criterion and one based on physical avoidability, rather than the development of a detection algorithm validated against ground truth. To nevertheless provide a quantitative assessment, additional indicators have been introduced, such as the temporal difference $\Delta TTC = TTC_{PONR} - TTC_{min}$ and the analysis of the relative timing of the PONR threshold with respect to critical TTC conditions. These indicators allow quantifying the advance provided by PONR compared to TTC.

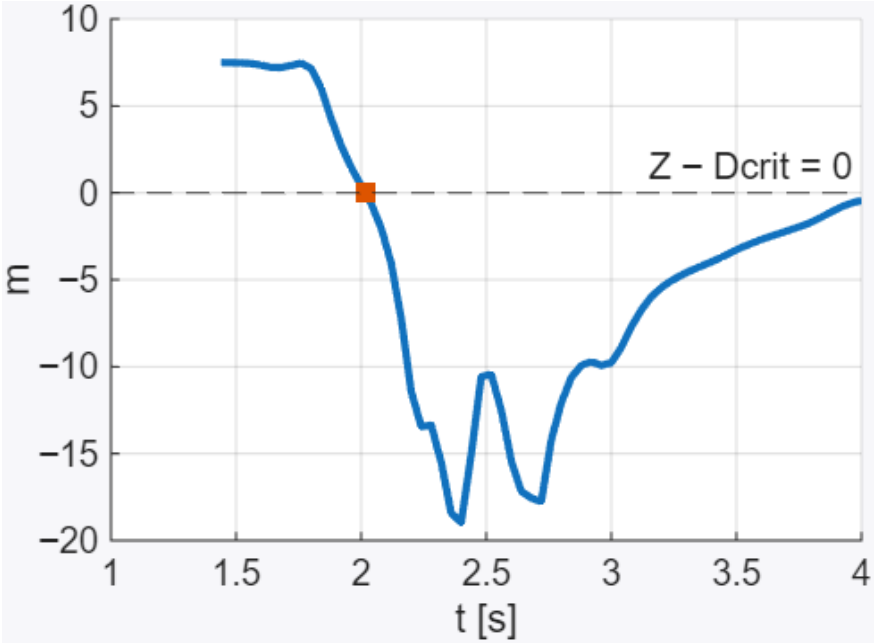

Figure 14. Temporal evolution of the PONR margin (extracted from real test).

It is important to note that the definition of classical metrics, such as detection accuracy or false positives, is limited in this context, as there is no direct ground truth for the moment of "collision inevitability," which depends on physical constraints and dynamic conditions.

Advanced surrogate safety measures based on fuzzy logic and multi-dimensional interactions have been proposed to better capture crash risk under uncertainty [45]. Furthermore, adaptive forward collision warning systems incorporate driver behaviour and risk levels to improve warning effectiveness. In addition, recent studies emphasize the importance of modelling driver responses to ADAS warnings, highlighting variability across behavioural profiles [46,47]. In contrast, the proposed PONR is a physically grounded threshold derived from braking capability, reaction time, and available distance, providing a deterministic boundary of collision inevitability. Unlike empirical or behaviour-based indicators, PONR does not rely on calibration to specific datasets or driver models but directly reflects the physical feasibility of collision avoidance, making it a complementary reference for evaluating and interpreting existing surrogate safety measures.

The results indicate that PONR can act as a complementary indicator to TTC in advanced driver assistance systems by explicitly identifying the transition to collision inevitability. Unlike TTC, which provides a continuous kinematic estimate, PONR introduces a physically grounded threshold that incorporates braking capability and available distance. From a system design perspective, this enables more timely and interpretable intervention strategies, while reducing sensitivity to transient fluctuations.

The proposed framework is intended as a proof-of-concept demonstration of the PONR indicator and, as such, presents several limitations. The methodology relies on monocular vision for distance estimation, which is sensitive to camera calibration, perspective effects, detection noise, and challenging conditions such as occlusions, illumination changes, or temporary detection failures. In addition, the relative speed is obtained through numerical differentiation, which may introduce fluctuations despite filtering. However, the objective of this study is not to evaluate the robustness of monocular perception itself but to demonstrate and analyze the PONR concept in comparison with TTC within a perception-driven pipeline. In this context, the monocular approach serves as an illustrative implementation based on widely available sensors. The proposed methodology is not inherently tied to monocular vision and can be extended to integrate more robust sensing

modalities, such as radar or LiDAR, which would improve distance and relative speed estimation in real-world conditions. Therefore, the conclusions regarding the comparative behaviour of TTC and PONR remain valid beyond the specific sensing configuration used in this study.

Furthermore, the analysis is limited to longitudinal rear-end scenarios and does not cover more complex traffic interactions. Finally, the framework has not been validated against high-precision ground-truth data or alternative sensing systems, and therefore primarily demonstrates the conceptual applicability of the PONR indicator.

5. Conclusions and Future Work

The results of this study consistently show that the Point of No Return (PONR) is reached earlier than the minimum time to collision (TTC) and provides a more stable and physically interpretable indication of collision inevitability. By explicitly incorporating braking capability and reaction constraints, PONR defines a clear boundary between avoidable and unavoidable states that cannot be captured by TTC alone. Within the proposed monocular vision framework, the experimental analysis confirms that PONR offers a more consistent characterization of critical situations across varying relative speeds.

This study is intended as a proof-of-concept demonstration of the PONR indicator rather than a fully validated perception or control framework. Nevertheless, the results highlight the potential of PONR as a complementary and forward-looking metric for collision risk assessment, supporting its relevance for future ADAS and collision avoidance strategies.

Future work should focus on validating the proposed approach against ground-truth distance measurements, extending the analysis to more complex multi-object scenarios, and incorporating more detailed vehicle dynamics models to improve braking capability estimation. By improving early risk detection and supporting safer vehicle interactions, PONR can contribute to sustainable urban mobility through enhanced traffic safety, smoother traffic flow, and reduced environmental impact

In addition, the integration of V2V and V2X communication represents a promising direction for enhancing PONR-based safety assessment. By enabling the exchange of vehicle states, motion intent, and real-time road friction estimates derived from onboard systems or infrastructure, PONR could be dynamically adapted to actual driving conditions, moving beyond conservative assumptions and improving the accuracy of collision inevitability prediction.

Although the current formulation does not explicitly incorporate real-time adaptation to changing road conditions, the proposed framework can be extended to support such functionality. In particular, the effective deceleration term used in the computation of the critical distance could be dynamically updated based on online estimates of tire–road friction. This would allow the PONR threshold to adapt to varying adhesion conditions, such as dry, wet, or low-friction surfaces. The integration of friction estimation techniques or slip-based control strategies represents a promising direction for enhancing the real-time applicability of the method.

Such cooperative extensions would allow PONR to evolve from a purely perception-based indicator to a shared, context-aware safety boundary within connected ADAS environments. Furthermore, the potential use of this concept as an early trigger for safety systems, such as a restraint pretensioner, should be investigated to assess its effectiveness compared to conventional TTC-based strategies.

Funding: This research received no external funding.

Institutional Review Board Statement: Not applicable.

Informed Consent Statement: Not applicable.

Data Availability Statement: Data is contained within this article.

Conflicts of Interest: The author declares no conflicts of interest.

References

1. Yang, L.; Yang, Y.; Wu, G.; Zhao, X.; Fang, S.; Liao, X.; Wang, R.; Zhang, M. A Systematic Review of Autonomous Emergency Braking System: Impact Factor, Technology, and Performance Evaluation. *J. Adv. Transp.* **2022**, *2022*, 1188089. [CrossRef]
2. Hoffmann, E.R.; Mortimer, R.G. Drivers' Estimates of Time to Collision. *Accid. Anal. Prev.* **1994**, *26*, 511–520. [CrossRef] [PubMed]
3. Ramezani Khansari, E.; Moghadas Nejad, F.; Moogehi, S. Comparing Time to Collision and Time Headway as Safety Criteria. *Pamukkale J. Eng. Sci.* **2021**, *27*, 669–675. [CrossRef]
4. Wessels, M.; Zähme, C.; Oberfeld, D. Auditory Information Improves Time-to-Collision Estimation for Accelerating Vehicles. *Curr. Psychol.* **2023**, *42*, 23195–23205. [CrossRef]
5. Li, Y.; Wu, D.; Lee, J.; Yang, M.; Shi, Y. Analysis of the Transition Condition of Rear-End Collisions Using Time-to-Collision Index and Vehicle Trajectory Data. *Accid. Anal. Prev.* **2020**, *144*, 105676. [CrossRef] [PubMed]
6. Automatic Emergency Braking Using a Time-to-Collision Threshold Based on Target Acceleration. Available online: https://patents.justia.com/patent/11724673 (accessed on 23 March 2026).
7. Kim, T.; Jeong, H.-Y. A Novel Algorithm for Crash Detection Under General Road Scenes Using Crash Probabilities and an Interactive Multiple Model Particle Filter. *IEEE Trans. Intell. Transport. Syst.* **2014**, *15*, 2480–2490. [CrossRef]
8. Meléndez-Useros, M.; Jiménez-Salas, M.; Viadero-Monasterio, F.; Boada, B.L. Tire Slip H∞ Control for Optimal Braking Depending on Road Condition. *Sensors* **2023**, *23*, 1417. [CrossRef]
9. Pretagostini, F.; Ferranti, L.; Berardo, G.; Ivanov, V.; Shyrokau, B. Survey on Wheel Slip Control Design Strategies, Evaluation and Application to Antilock Braking Systems. *IEEE Access* **2020**, *8*, 10951–10970. [CrossRef]
10. Wang, D.; Liu, S.; Wei, X.; He, Y. A Wheel Slip Ratio Constraint Control for ABS Based on Tangent Type Barrier Lyapunov Function. *Meas. Control* **2023**, *56*, 411–419. [CrossRef]
11. Crocetti, F.; Costante, G.; Fravolini, M.L.; Valigi, P. A Data-Driven Slip Estimation Approach for Effective Braking Control under Varying Road Conditions. In *Proceedings of the 2020 28th Mediterranean Conference on Control and Automation (MED), Saint-Raphaël, France, 15–18 September 2020*; IEEE: New York, NY, USA, 2020; pp. 496–501.
12. Park, K.-Y.; Hwang, S.-Y. Robust Range Estimation with a Monocular Camera for Vision-Based Forward Collision Warning System. *Sci. World J.* **2014**, *2014*, 923632. [CrossRef]
13. Han, J.; Heo, O.; Park, M.; Kee, S.; Sunwoo, M. Vehicle Distance Estimation Using a Mono-Camera for FCW/AEB Systems. *Int.J. Automot. Technol.* **2016**, *17*, 483–491. [CrossRef]
14. Dellaert, F.; Thorpe, C. Robust Car Tracking Using Kalman filtering and Bayesian Templates. In Proceedings of the 1997 Conference on Intelligent Transportation Systems, Boston, MA, USA, 9–12 November 1997.
15. Gao, J.; Han, G.; Zhu, H.; Liao, L. Multiple Moving Vehicles Tracking Algorithm with Attention Mechanism and Motion Model. *Electronics* **2024**, *13*, 242. [CrossRef]
16. Taylor, L.E.; Mirdanies, M.; Saputra, R.P. Optimized Object Tracking Technique Using Kalman Filter. *J. Mechatron. Electr. Power Veh. Technol.* **2016**, *7*, 57–66. [CrossRef]
17. Lee, S.; Han, K.; Park, S.; Yang, X. Vehicle Distance Estimation from a Monocular Camera for Advanced Driver Assistance Systems. *Symmetry* **2022**, *14*, 2657. [CrossRef]
18. Megalingam, R.K.; Shriram, V.; Likhith, B.; Rajesh, G.; Ghanta, S. Monocular Distance Estimation Using Pinhole Camera Approximation to Avoid Vehicle Crash and Back-over Accidents. In *Proceedings of the 2016 10th International Conference on Intelligent Systems and Control (ISCO), Coimbatore, India, 7–8 January 2016*; IEEE: New York, NY, USA; pp. 1–5.
19. Agand, P.; Chang, M.; Chen, M. DMODE: Differential Monocular Object Distance Estimation Module without Class Specific Information. In *Proceedings of the 2024 13th International Workshop on Robot Motion and Control (RoMoCo)*; IEEE: New York, NY, USA, 2024.
20. Mamduhi, M.H.; Hashemi, E.; Baras, J.S.; Johansson, K.H. Event-Triggered Add-on Safety for Connected and Automated Vehicles Using Road-Side Network Infrastructure. *IFAC-Pap.* **2020**, *53*, 15154–15160. [CrossRef]
21. Yimer, T.H.; Wen, C.; Yu, X.; Jiang, C. A Study of the Minimum Safe Distance between Human Driven and Driverless Cars Using Safe Distance Model. *arXiv* **2020**, arXiv:2006.07022. [CrossRef]
22. Hayward, J.C. Near-Miss Determination Through Use of a Scale of Danger. *Highw. Res. Rec.* **1972**, *384*, 24–35.
23. Lai, F.; Liu, J.; Hu, Y. An Automatic Emergency Braking Control Method for Improving Ride Comfort. *World Electr. Veh. J.* **2024**, *15*, 259. [CrossRef]
24. Chen, T.; Liu, K.; Wang, Z.; Deng, G.; Chen, B. Vehicle Forward Collision Warning Algorithm Based on Road Friction. *Transp. Res. Part D Transp. Environ.* **2019**, *66*, 49–57. [CrossRef]

25. Pak, J.M. Hybrid Interacting Multiple Model Filtering for Improving the Reliability of Radar-Based Forward Collision Warning Systems. *Sensors* **2022**, *22*, 875. [CrossRef] [PubMed]
26. Yang, X.; Lubbe, N.; Bärgman, J. Evaluation of Comfort Zone Boundary Based Automated Emergency Braking Algorithms for Car-to-powered-two-wheeler Crashes in China. *IET Intell. Transp. Syst.* **2024**, *18*, 1599–1615. [CrossRef]
27. Shalev-Shwartz, S.; Shammah, S.; Shashua, A. On a Formal Model of Safe and Scalable Self-Driving Cars. *arXiv* **2018**, arXiv:1708.06374. [CrossRef]
28. Spitzhüttl, F.; Liers, H. Calculation of the Point of No Return (PONR) from Real-World Accidents. In Proceedings of the 26th International Technical Conference on the Enhanced Safety of Vehicles (ESV): Technology: Enabling a Safer Tomorrow, National Highway Traffic Safety Administration, Eindhoven, The Netherlands, 10–13 June 2019.
29. Ma, X.; Yu, Q.; Liu, J. Modeling Urban Freeway Rear-End Collision Risk Using Machine Learning Algorithms. *Sustainability* **2022**, *14*, 12047. [CrossRef]
30. What Is Camera Calibration? Available online: https://www.mathworks.com/help/vision/ug/camera-calibration.html (accessed on 23 March 2026).
31. Camera Calibration and 3D Reconstruction. Available online: https://docs.opencv.org/4.x/d9/d0c/group__calib3d.html (accessed on 23 March 2026).
32. Redmon, J.; Divvala, S.; Girshick, R.; Farhadi, A. You Only Look Once: Unified, Real-Time Object Detection. In Proceedings of the 2016 IEEE Conference on Computer Vision and Pattern Recognition (CVPR), Las Vegas, NV, USA, 27–30 June 2016.
33. Zhang, A.; Lipton, Z.C.; Li, M.; Smola, A.J. *Dive into Deep Learning*; Online Book; Cambridge University Press: Cambridge, UK, 2023.
34. Murat, A.A.; Kiran, M.S. A Comprehensive Review on YOLO Versions for Object Detection. *Eng. Sci. Technol. Int. J.* **2025**, *70*, 102161. [CrossRef]
35. Liang, H.; Ma, Z.; Zhang, Q. Self-Supervised Object Distance Estimation Using a Monocular Camera. *Sensors* **2022**, *22*, 2936. [CrossRef] [PubMed]
36. Shi, X.; Ye, Q.; Chen, X.; Chen, C.; Chen, Z.; Kim, T.-K. Geometry-Based Distance Decomposition for Monocular 3D Object Detection. In Proceedings of the IEEE/CVF International Conference on Computer Vision, New Orleans, LA, USA, 18–24 June 2022.
37. Elsagheer Mohamed, S.A.; Alshalfan, K.A.; Al-Hagery, M.A.; Ben Othman, M.T. Safe Driving Distance and Speed for Collision Avoidance in Connected Vehicles. *Sensors* **2022**, *22*, 7051. [CrossRef]
38. Samson, C.J.R.; Hussain, Q.; Alhajyaseen, W.K.M. Analysis of Stopping Sight Distance (SSD) Parameters: A Review Study. *Procedia Comput. Sci.* **2022**, *201*, 126–133. [CrossRef]
39. Meywerk, M. *Vehicle Dynamics*; John Wiley & Sons Ltd.: Hoboken, NJ, USA, 2015; ISBN 978-1-118-97135-2.
40. Haus, S.H.; Sherony, R.; Gabler, H.C. Estimated Benefit of Automated Emergency Braking Systems for Vehicle–Pedestrian Crashes in the United States. *Traffic Inj. Prev.* **2019**, *20*, S171–S176. [CrossRef] [PubMed]
41. Karimi, A.; Mirza Boroujerdian, A.; Amini, I. Risk Evaluation of Multiple Passing Maneuvers on Two-Lane Rural Highways in Iran. *Accid. Anal. Prev.* **2021**, *163*, 106472. [CrossRef] [PubMed]
42. Zimmermann, J.; Mönnich, J.; Scherl, M.; Llatser, I.; Wildschütte, F.; Hofmann, F. Analyzing the Performance of a V2X-Enhanced Braking System in Real-World Crash Situations. In *Proceedings of the 2025 IEEE Vehicular Networking Conference (VNC), Porto, Portugal, 2–4 June 2025*; IEEE: New York, NY, USA, 2025; pp. 1–8.
43. Wagner, S.; Groh, K.; Kuhbeck, T.; Dorfel, M.; Knoll, A. Using Time-to-React Based on Naturalistic Traffic Object Behavior for Scenario-Based Risk Assessment of Automated Driving. In *Proceedings of the 2018 IEEE Intelligent Vehicles Symposium (IV), Changshu, 26–30 June 2018*; IEEE: New York, NY, USA, 2018; pp. 1521–1528.
44. Road Friction Estimation: Why Real-Time Edge Computing Is Redefining Autonomous Vehicle Safety in 2026. Available online: https://www.easyrain.it/road-friction-estimation/ (accessed on 23 March 2026).
45. Xu, Y.; Ye, W.; Xie, Y.; Wang, C. A Two-Dimensional Surrogate Safety Measure Based on Fuzzy Logic Model. *Accid. Anal. Prev.* **2024**, *199*, 107529. [CrossRef]
46. Shao, Y.; Shi, X.; Zhang, Y.; Zhang, Y.; Xu, Y.; Chen, W.; Ye, Z. Adaptive Forward Collision Warning System for Hazmat Truck Drivers: Considering Differential Driving Behavior and Risk Levels. *Accid. Anal. Prev.* **2023**, *191*, 107221. [CrossRef] [PubMed]
47. Shao, Y.; Xu, Y.; Ye, Z.; Zhang, Y.; Chen, W.; Shiwakoti, N.; Shi, X. Understanding the Impacts of Negative Advanced Driving Assistance System Warnings on Hazardous Materials Truck Drivers' Responses Using Interpretable Machine Learning. *Eng. Appl. Artif. Intell.* **2025**, *146*, 110308. [CrossRef]